NATIONAL ADVISORY COMMITTEE FOR AERONAUTICS

WARTIME REPORT

ORIGINALLY ISSUED

November 1945 as
Advance Confidential Report L5G10

EFFECTS OF COMPRESSIBILITY ON THE MAXIMUM LIFT CHARACTERISTICS AND SPANWISE LOAD DISTRIBUTION OF A 12-FOOT-SPAN FIGHTER-TYPE WING OF NACA 230-SERIES AIRFOIL SECTIONS

By E. O. Pearson, Jr., A. J. Evans
and F. E. West, Jr.

Langley Memorial Aeronautical Laboratory
Langley Field, Va.

WASHINGTON

NACA ACR No. L5G10

NATIONAL ADVISORY COMMITTEE FOR AERONAUTICS

ADVANCE CONFIDENTIAL REPORT

EFFECTS OF COMPRESSIBILITY ON THE MAXIMUM LIFT CHARACTERISTICS AND SPANWISE LOAD DISTRIBUTION OF A 12-FOOT-SPAN FIGHTER-TYPE WING OF NACA 230-SERIES AIRFOIL SECTIONS

By E. O. Pearson, Jr., A. J. Evans
and F. E. West, Jr.

SUMMARY

Force and pressure-distribution measurements were made on a fighter-type wing model of conventional NACA 230-series airfoil sections in the Langley 16-foot high-speed tunnel to determine the effects of compressibility on the maximum lift characteristics and the spanwise load distribution. The range of angle of attack investigated was from -10° to 24°. The Mach number range was from 0.20 to 0.70 at small and medium angles of attack and from 0.15 to 0.625 at very large angles of attack.

In the Mach number range from 0.15 to 0.55, the maximum lift coefficient first increased with increasing Mach number and then decreased rapidly after having reached a peak value at a Mach number of 0.30. At Mach numbers higher than 0.55, the rate of decrease of maximum lift coefficient with Mach number was considerably reduced. At these higher speeds the lift coefficient continued to increase with angle of attack well beyond the angle at which marked flow separation or stalling occurred, and the maximum lift coefficient was reached at angles 10° to 12° beyond the stalling angle.

No significant changes in the span load distribution were found to occur below the stall at any of the test speeds. When the wing stalled at high speeds, the resultant load underwent a moderate outboard shift, which resulted in increases in root bending moment up to about 10 percent.

INTRODUCTION

Wind-tunnel tests of a rectangular wing of NACA 0012 airfoil section (reference 1) showed that the maximum lift coefficient reached a peak value at the low Mach number of 0.19 and decreased rapidly as the Mach number M was increased from this value up to the highest Mach number of the tests (M ≈ 0.35). Although these tests were necessarily limited in scope, they indicated the importance of a knowledge of the effect of compressibility on the maximum lift coefficient both in the estimation of the maneuvering performance and loads of high-speed aircraft and in the interpretation of wind-tunnel maximum lift data as applied to the prediction of airplane characteristics at low speeds.

More recent two-dimensional wind-tunnel tests of a number of propeller-type airfoils over a relatively large Mach number range (reference 2) showed effects for the thicker airfoils similar to those of reference 1 and in addition showed large increases in the maximum lift coefficient starting at Mach numbers of about 0.5. Flight tests of fighter airplanes reported in references 3 and 4 showed large decreases in the lift coefficient corresponding to the stall up to Mach numbers of about 0.6.

A high-speed wind-tunnel investigation of a number of three-dimensional wings of different airfoil sections has been undertaken to provide more detailed information on the high-speed stalling phenomena. Measurements to determine the effect of compressibility on the spanwise load distribution were included in the program because of the related importance of the load distribution as a determining factor of the strength requirements of wings. The present report gives the preliminary results of force and pressure measurements in the Langley 16-foot high-speed tunnel on the first of a series of wings. The model tested was a fighter-type wing having an aspect ratio of 6, a taper ratio of 2:1, and conventional NACA 230-series airfoil sections.

[redacted]

SYMBOLS

V	true airspeed, feet per second
a	speed of sound in air, feet per second
M	Mach number (V/a)
ρ	air density, slugs per cubic foot
q	dynamic pressure, pounds per square foot $\left(\frac{1}{2}\rho V^2\right)$
R	Reynolds number $\left(\frac{\rho \bar{c} V}{\mu}\right)$
μ	coefficient of viscosity of air, slugs per foot-second

The foregoing symbols represent the undisturbed stream values.

C	cross-sectional area of the tunnel at the throat, square feet
D	equivalent diameter of the tunnel test section, feet $\left(\sqrt{\frac{4C}{\pi}}\right)$
S	wing area, square feet
b	wing span, feet
y	spanwise distance measured from the plane of symmetry, feet
c_s	airfoil chord at plane of symmetry, feet
$\bar{c}$	mean chord, feet (S/b)
c	airfoil chord at any spanwise location, feet
t	maximum thickness of airfoil section corresponding to the mean chord, feet

[redacted]

L wing lift, pounds

C_L wing lift coefficient $\left(\frac{L}{qS}\right)$

n section normal force (force per unit span), pounds per foot

c_n section normal-force coefficient $\left(\frac{n}{qc}\right)$

$c_n \frac{c}{c_s}$ load coefficient

C_N wing normal-force coefficient $\left(2 \frac{c_s}{S} \int_0^{\frac{b}{2}} c_n \frac{c}{c_s} dy\right)$

α corrected angle of attack of the root section (section at the plane of symmetry), degrees

$\Delta\alpha_{LL}$ angle-of-attack correction due to the jet boundary-induced upwash at the lifting line, degrees $\left(57.3 \delta \frac{S}{C} C_L\right)$

δ a function of the ratio of wing span to tunnel diameter $\left(\frac{1}{8}\left[1 + \frac{3}{16}\left(\frac{b}{D}\right)^4 + \frac{5}{64}\left(\frac{b}{D}\right)^8 + \cdots\right]\right)$

$\Delta\alpha_{SC}$ angle-of-attack correction due to the jet boundary-induced streamline curvature, degrees $\left(\frac{1.05}{\sqrt{1 - M^2}} \frac{\bar{c}}{D} \Delta\alpha_{LL}\right)$

APPARATUS AND METHODS

A diagrammatic sketch of the wing model used in the tests is given in figure 1. The principal dimensions given in the figure and other pertinent information are given in the following list:

[redacted]

Span, ft	12
Area, sq ft	24
Aspect ratio	6
Taper ratio	2:1
Geometric and aerodynamic twist (washout), deg	4.2
Root section	NACA 23016
Tip section	NACA 23009
Dihedral (along the 1/4 chord line), deg	0
Sweepback (along the 1/4 chord line), deg	3.18

The wing was of built-up steel construction and was machined in such a manner that surface elements connecting equal percentage-chord points of the root and tip sections were straight lines.

Thirty-three pressure orifices were distributed over each of six wing sections, the spanwise locations of which are given in figure 1. The chordwise distribution of pressure orifices for a typical section is also shown in figure 1. The pressure tubes were brought out of the wing to multiple-tube manometers in the test chamber by means of the boom and movable strut arrangement shown in figure 2. For the force tests the boom and strut were removed and the boom replaced with a short fairing, which is shown in figure 1.

The wing was mounted at the tunnel center line on shielded struts having a thickness-chord ratio of 0.15. The thickness-chord ratio of the shields was 0.124. Figure 3 is a photograph of the wing mounted upright in the tunnel for the force tests.

Most of the test runs were made with the angle of attack held constant while the tunnel speed was varied from about 150 miles per hour to the maximum speed obtainable, which for wing angles of attack between 0° and 4° was approximately 520 miles per hour. The corresponding Mach number range was from 0.20 to 0.70, and the corresponding range of average Reynolds number was from 3.0×10^6 to 8.1×10^6. Figure 4 shows the variation of average Reynolds number with Mach number. For very large wing angles of attack the maximum obtainable tunnel speed was about 460 miles per hour, which corresponds to a Mach number of about 0.625. In the determination of maximum lift coefficients additional tests were made with the tunnel speed held constant while the angle of attack was varied in the region near maximum lift. The geometric angle-of-attack range of the tests was from -10° to 24°.

[redacted]

In the load-distribution tests the static pressures over the six wing sections, as indicated by several multiple-tube manometers, were recorded photographically. The chordwise pressure distributions determined from these photographic records were integrated mechanically to find the section normal-force coefficients.

CORRECTIONS

Force data.- The force data have been corrected for strut tares, air-stream misalinement, and tunnel-wall effects.

The strut tare forces were determined from tests with the wing inverted with and without image support struts installed. A photograph of the inverted wing with the image struts installed is given in figure 8. The largest increments of lift coefficient due to the support struts were between 0.03 and 0.04.

The effective misalinement angle of the air stream was determined from tests of the wing upright and inverted with the image struts installed and was found to be constant at 0.15° throughout the speed range of the tests.

In order to prevent air leakage through the strut shields, thin rubber diaphragms were fitted around the bases of the shields. An additional correction to the lift was necessitated because of a pressure differential across the diaphragms. This pressure differential was measured during the force tests by means of a micromanometer, and a calibration was made with the wing removed to determine the variation of lift force with pressure differential. This correction was very small in the region of maximum lift (less than one-half of 1 percent at all speeds).

The effects of the tunnel walls were accounted for by the methods of references 5, 6, and 7 as follows: The principal part of the angle-of-attack correction given in reference 5 is

$$\Delta\alpha_{LL} = 57.36 \frac{S}{C} C_L \text{ degrees}$$

This equation is strictly valid only for the case of an elliptical spanwise load distribution. A check calculation

[redacted]

by a more exact but more detailed procedure based on the experimentally determined span loading revealed that the error incurred by the use of the simpler form was negligible. At a wing lift coefficient of 1.0 the correction was 0.93°.

An additional correction to the angle of attack due to an induced curvature of the flow was calculated from the equation

$$\Delta\alpha_{SC} = \frac{1.05}{\sqrt{1 - M^2}} \frac{\bar{c}}{D} \Delta\alpha_{LL}$$

This equation is based on the original incompressible-flow derivation of reference 6. The modification $\sqrt{1 - M^2}$ is given in reference 5. This correction amounted to 0.16° at a lift coefficient of 1.0 and a Mach number of 0.6.

Corrections to the stream velocity, dynamic pressure, and Mach number, and to the wing lift coefficient due to constriction effects were calculated by the method of reference 7. The correction to the velocity is

$$\frac{\Delta V}{V} = \frac{0.6b\bar{c}t}{(BH)^{3/2}\left(\sqrt{1 - M^2}\right)^3} + \frac{C_{D_o}\bar{c}}{4H\left(\sqrt{1 - M^2}\right)^2}$$

where ΔV is the effective incremental velocity due to constriction, B and H are the breadth and height of a rectangular tunnel, and C_{D_o} is the wing profile-drag coefficient. The two terms on the right of the equation give the velocity increments due, respectively, to "solid" constriction and "wake" constriction. Since the magnitude of the wake constriction effect is a function of the velocity loss in the wake and the size of the wake, the correction is expressed in terms of the profile-drag coefficient, which is also a function of those quantities.

No theoretical treatment of the problem of constriction effects for a finite wing in a circular tunnel exists at the present time, and the foregoing relation was thought to represent the best available approximation. As modified for the case of the circular tunnel, the equation became

$$\frac{\Delta V}{V} = \frac{0.6b\bar{c}t}{C^{3/2}\left(\sqrt{1 - M^2}\right)^3} + \frac{C_{D_o}\bar{c}}{4H\left(\sqrt{1 - M^2}\right)^2}$$

[redacted]

where H in this case is the average height of the tunnel in the region occupied by the wing. The constriction corrections to the dynamic pressure, Mach number (reference 5), and wing lift coefficient are as follows:

$$\frac{\Delta q}{q} = 2\frac{\Delta V}{V}$$

$$\frac{\Delta M}{M} = \left(1 + 0.2M^2\right)\frac{\Delta V}{V}$$

$$\frac{-\Delta C_L}{C_L} = \frac{\Delta q}{q}$$

The corrections were small for low angles of attack over the entire Mach number range. At a geometric angle of attack of 4° and a Mach number of 0.7 the corrections to the lift coefficient and Mach number were, respectively, 1.0 percent and 0.6 percent. At angles of attack above the stall where the drag became very large (indicative of a large wake), the corrections assumed some importance. At a geometric angle of attack of 24° and a Mach number of 0.6 the corrections to the lift coefficient and Mach number were 4.2 percent and 2.2 percent, respectively.

Pressure-distribution data.- The pressure-distribution data have been corrected for the principal effects of the support struts in that the free-stream values of static pressure and dynamic pressure upon which the pressure coefficients were based were determined from a survey of the flow in the test section with the support struts and shields installed. Some small local effects of the struts on the spanwise load distribution remain. These effects will be discussed in the section entitled "Results and Discussion."

The effect of the tunnel walls on the spanwise load distribution was considered and found to be very small; consequently, these data as presented are uncorrected for tunnel-wall interference.

RESULTS AND DISCUSSION

Wing lift characteristics (force test results).- The lift characteristics of the wing as a function of angle

of attack and Mach number are shown in figures 6 and 7. Figure 6 is presented to indicate by the scatter of the test points the precision with which the data were obtained. The same data with the test-point symbols removed and with the horizontal lines drawn for constant and even values of angle of attack are given in figure 7.

The variation of maximum lift coefficient $C_{L_{max}}$ with Mach number is shown in figure 8. The maximum lift coefficient increases with increasing Mach number until a Mach number of about 0.30 is reached. This increase can probably be attributed to a combination of Reynolds number and Mach number effects; however, the Reynolds number effect probably predominates in this region. As the Mach number is increased above 0.30, the maximum lift coefficient decreases at an increasingly rapid rate until a Mach number of about 0.55 is reached. In the region between $M = 0.55$ and $M = 0.625$ the rate of decrease of maximum lift coefficient with Mach number is considerably reduced.

The lift-coefficient curves of figure 7 are presented again in figure 9, plotted to a common angle-of-attack scale to illustrate more clearly the changing character of the stall as the Mach number is increased. As the Mach number increases above 0.30 the angle of attack at which the wing stalls progressively decreases; also, at Mach numbers below 0.55 the stalling angle and the angle for maximum lift are approximately the same. At Mach numbers above 0.55, however, the maximum lift coefficient occurs at an angle of attack 10° to 12° higher than that at which pronounced separation of the flow begins.

These data indicate that for airplanes with wings similar to the test wing there exists at high speeds a range of maximum obtainable lift coefficient. This range extends from the lift coefficient corresponding to the initial stall (such as shown by the lower dashed curve of figure 8) to that corresponding to the actual maximum lift coefficient of the wing. At the lower value of lift coefficient corresponding to the change in slope of the lift curves of figure 9, increases in stability due primarily to decreases in downwash angle are likely to occur. It might be expected therefore that at high speeds the amount of elevator control available would be an important factor in determining the maximum lift coefficient obtainable (reference 4). Thus, an airplane with a limited amount of elevator control might be capable of reaching an angle of attack only a few

[redacted]

degrees above the stall, and the maximum lift coefficients obtainable might be only slightly greater than those represented by the lower dashed curve of figure 8. Tail buffeting is also likely to occur when the flow separates from the wing, so that piloting technique cannot be overlooked as a possible determining factor. Finally, at very high Mach numbers it is possible that actual instability might be encountered, in which case high angles of attack and high lifts might be obtained inadvertently regardless of the control power.

Spanwise load distribution.- Spanwise load distribution curves for a number of values of wing normal-force coefficient and Mach number are shown in figure 10. As mentioned previously the principal effect of the support struts (which is to increase the effective stream velocity) was accounted for by calibrating the tunnel with the struts installed. The local effect of the struts is to reduce the lift at a given angle of attack by a small amount and to produce a slight distortion in the span loading. This distortion may be seen as a dip in the curves of figure 10 near the spanwise station $\frac{y}{b/2} = 0.65$. The solid and dashed curves of figure 10 represent the load distributions before and after the stall, respectively.

The curves of figure 11 summarize the changes in span loading that were found to occur at the higher test speeds. No significant changes in the span loading were found to occur below the stall at any of the speeds of the test, even when shock waves were well established over the center part of the wing. Changes in the span loading were observed to take place above the high-speed stall, however, the center of load being shifted outboard. These changes at the higher speeds were found to be moderate. The largest corresponding increase in bending moment at the root (for constant lift) was found to be about 10 percent at a Mach number of 0.55 and a wing normal-force coefficient of about 0.95. The changes in load distribution due to stalling at low speeds were somewhat larger than those at high speeds but are not of particular significance because the total lift cannot be maintained beyond the stall.

A comparison of the experimentally determined load distribution curves at $M = 0.40$ with those calculated by the method of reference 8 is shown in figure 12 for values of wing normal-force coefficient of 0 and 1.0.

[redacted]

The agreement shown is typical of that existing in the unstalled part of the lift curves.

CONCLUDING REMARKS

Wind-tunnel tests of a tapered wing of NACA 230-series airfoil sections at Mach numbers ranging from 0.15 to 0.70 have shown that:

1. The maximum lift coefficient first increased with increasing Mach number up to a Mach number of 0.3. As the Mach number was increased above this value the maximum lift coefficient decreased rapidly.

2. A large reduction in the rate of decrease of maximum lift coefficient with Mach number occurred in the Mach number range of 0.55 to 0.625. The tunnel Mach number of 0.625 was the highest value that could be obtained at the large angles of attack requisite for maximum lift.

3. At Mach numbers below 0.55 the angles of attack at which the maximum lift coefficient was reached and at which stalling occurred were approximately the same. At Mach numbers above 0.55 the angle of attack at which the maximum lift coefficient was reached was 10° to 12° beyond the angle at which the wing initially stalled.

4. No significant changes in the span load distribution occurred below the stall at any of the speeds tested.

5. Moderate changes in the span load distribution occurred when the wing stalled at high speed, the center of load being shifted outboard. The largest corresponding increase in bending moment at the wing root for constant

[redacted]

lift was about 10 percent and occurred at a Mach number of 0.55 and at a wing normal-force coefficient of about 0.95.

Langley Memorial Aeronautical Laboratory
National Advisory Committee for Aeronautics
Langley Field, Va.

[redacted]

REFERENCES

1. Muse, Thomas C.: Some Effects of Reynolds and Mach Numbers on the Lift of an NACA 0012 Rectangular Wing in the NACA 19-Foot Pressure Tunnel. NACA CB No. 3E29, 1943.

2. Cleary, Harold E.: Effects of Compressibility on Maximum Lift Coefficients for Six Propeller Airfoils. NACA ACR No. L4L21a, 1945.

3. Rhode, Richard V.: Correlation of Flight Data on Limit Pressure Coefficients and Their Relation to High-Speed Burbling and Critical Tail Loads. NACA ACR No. L4I27, 1944.

4. Nissen, James M., and Gadeberg, Burnett L.: Effect of Mach and Reynolds Numbers on the Power-Off Maximum Lift Coefficient Obtainable on a P-39N-1 Airplane as Determined in Flight. NACA ACR No. 4F28, 1944.

5. Goldstein, S., and Young, A. D.: The Linear Perturbation Theory of Compressible Flow, with Applications to Wind-Tunnel Interference. R. & M. No. 1909, British A.R.C., 1943.

6. Lotz, Irmgard: Correction of Downwash in Wind Tunnels of Circular and Elliptic Sections. NACA TM No. 801, 1936.

7. Thom, A.: Blockage Corrections and Choking in the R.A.E. High Speed Tunnel. Rep. No. Aero 1891, British R.A.E., Nov. 1943.

8. Anon.: Spanwise Air-Load Distribution. ANC-1(1), Army-Navy-Commerce Committee on Aircraft Requirements. U. S. Govt. Printing Office, April 1938.

[redacted]

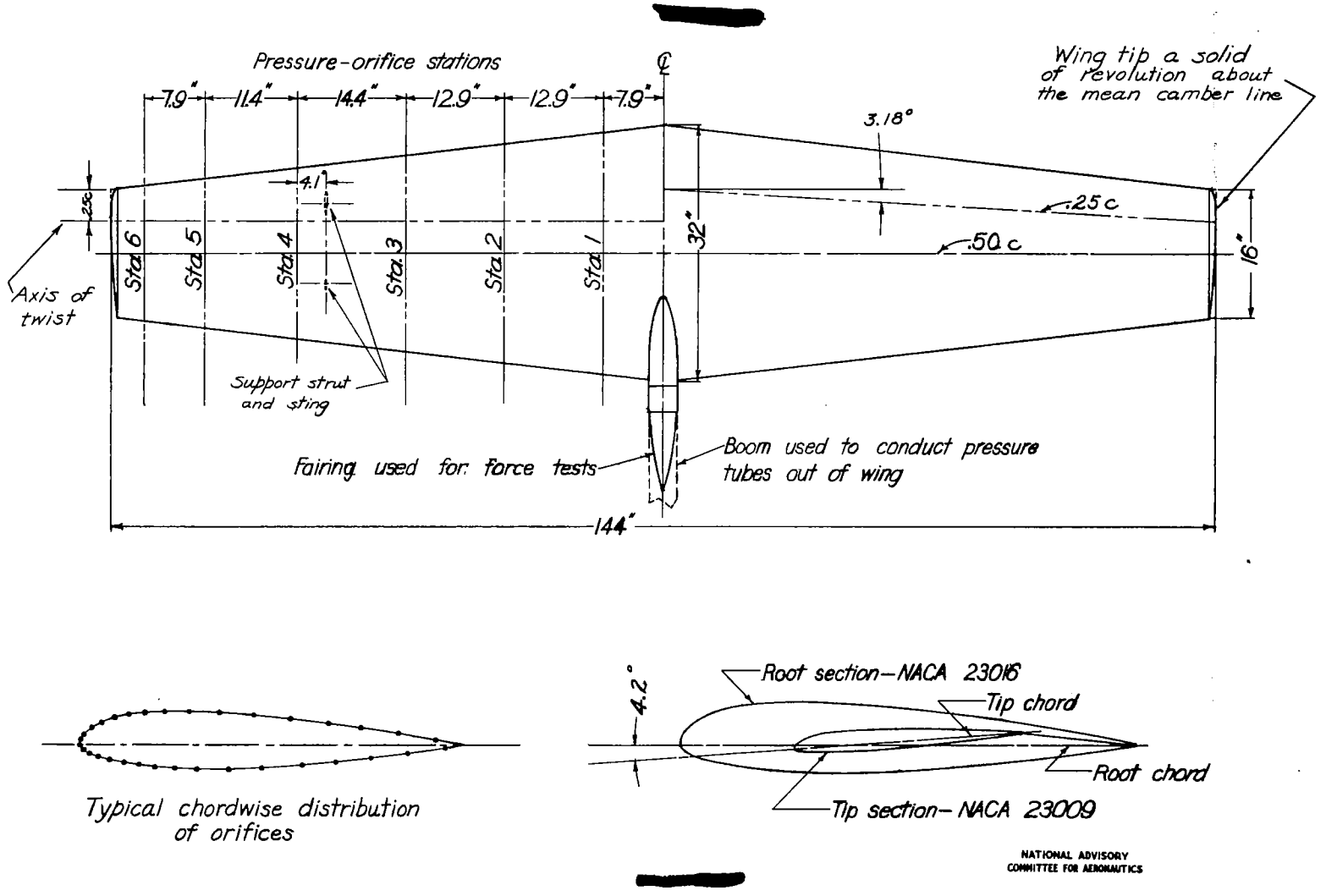

Figure 1.—Principal wing dimensions and locations of pressure orifices.

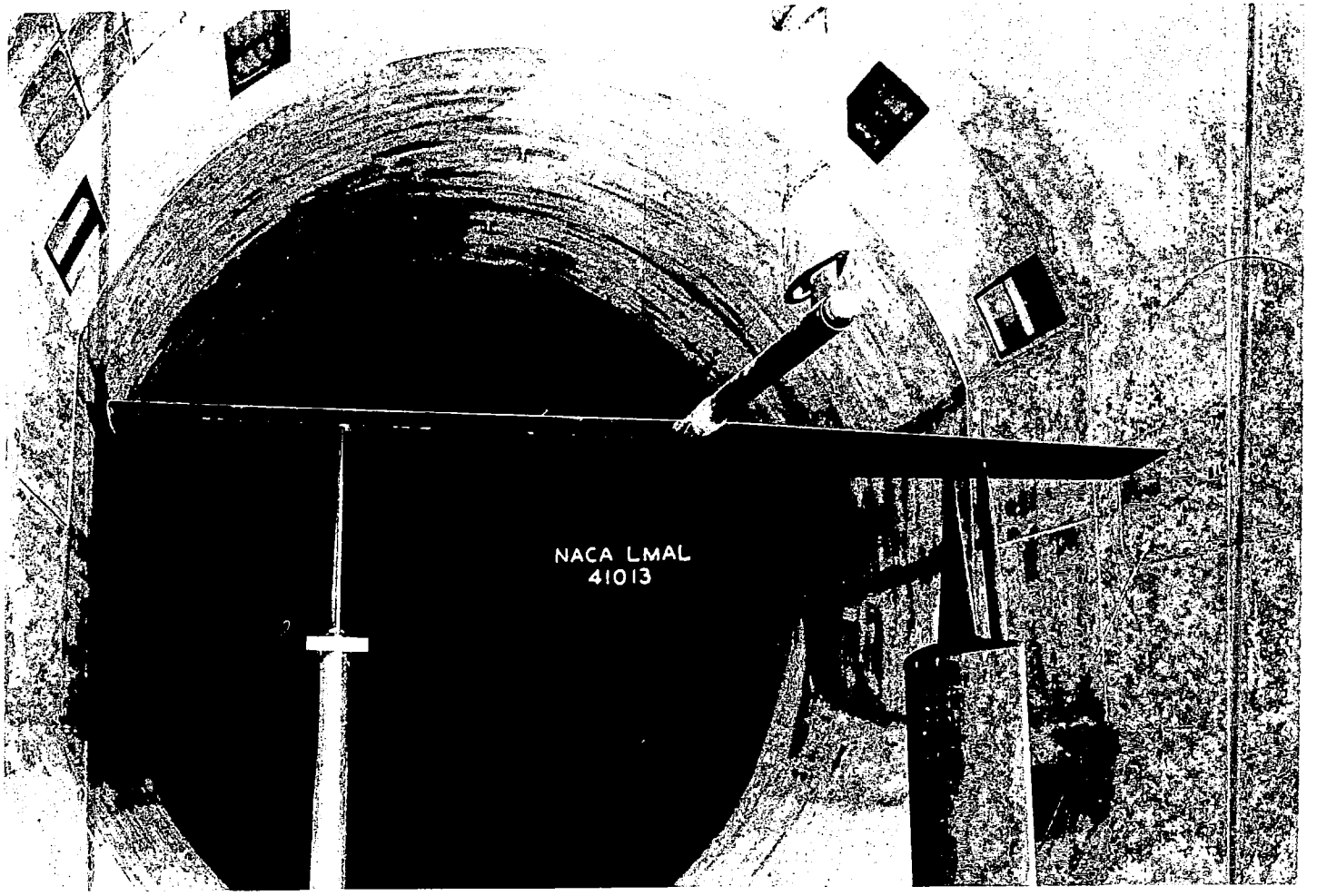

Figure 2.- Rear view of wing showing boom and strut assembly used to conduct pressure tubes to manometers.

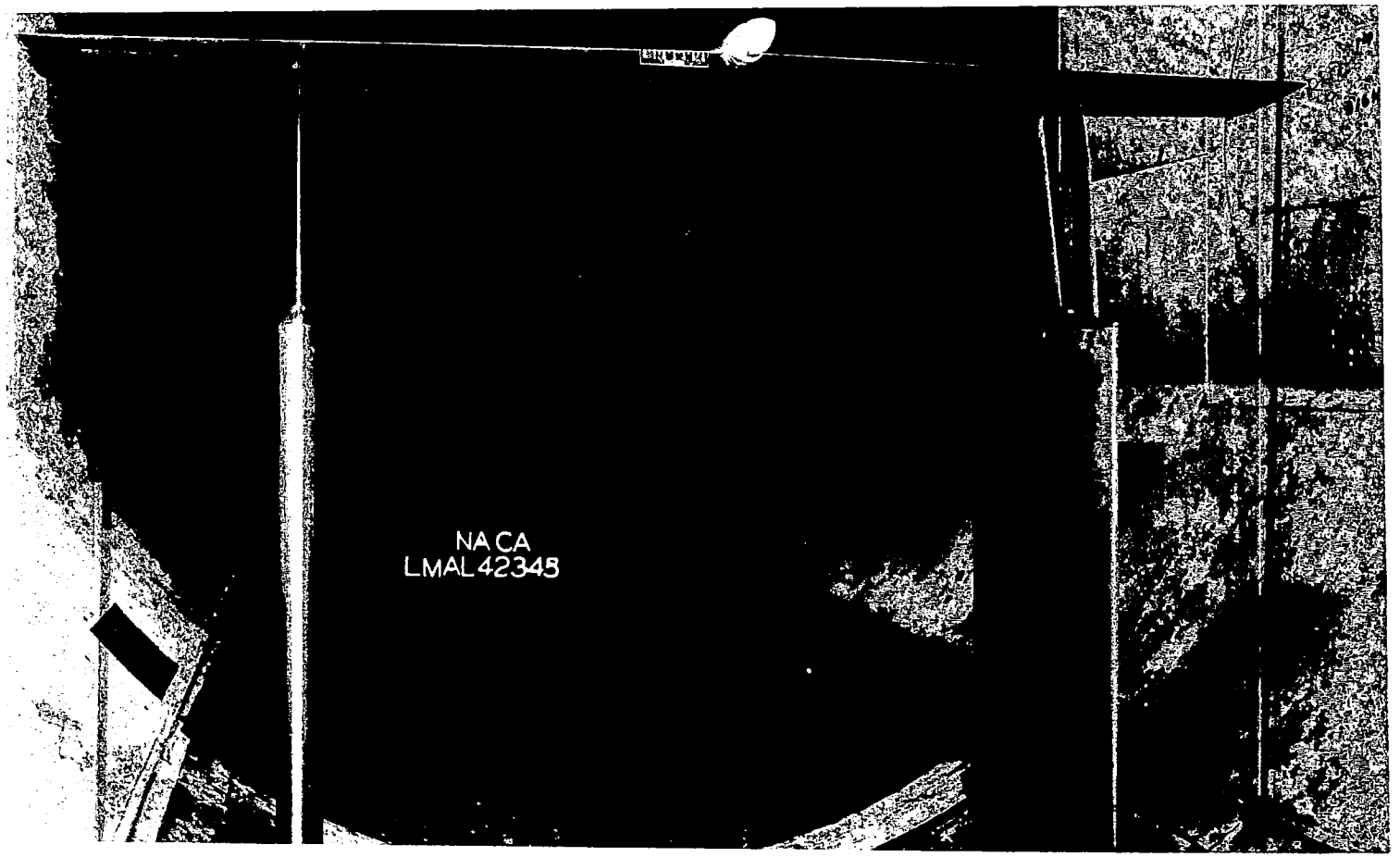

Figure 3.- Rear view of wing mounted upright in the tunnel for force measurements.

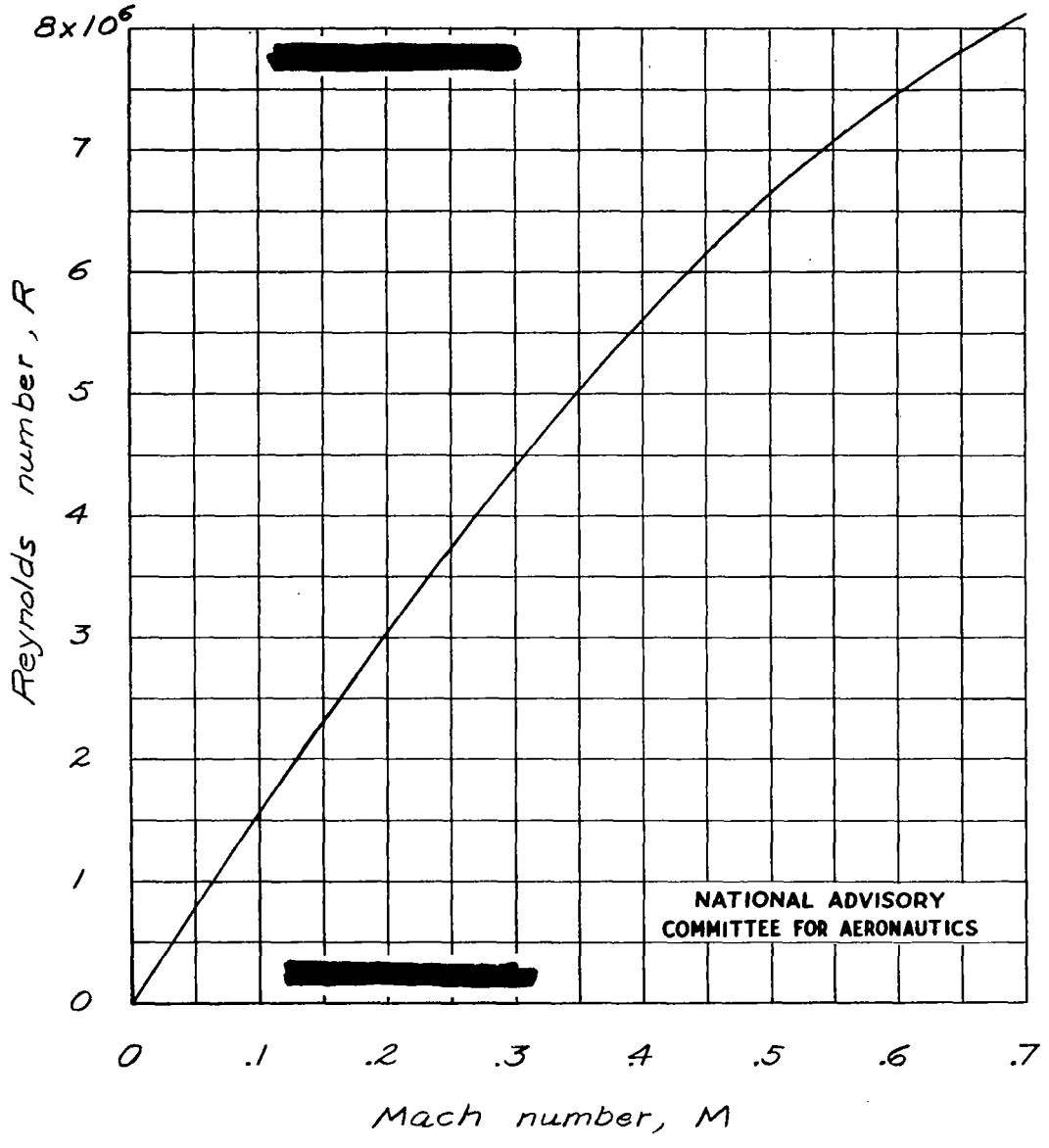

Figure 4.- Variation of average Reynolds number with Mach number.
$\bar{c}$ = 2.0 feet.

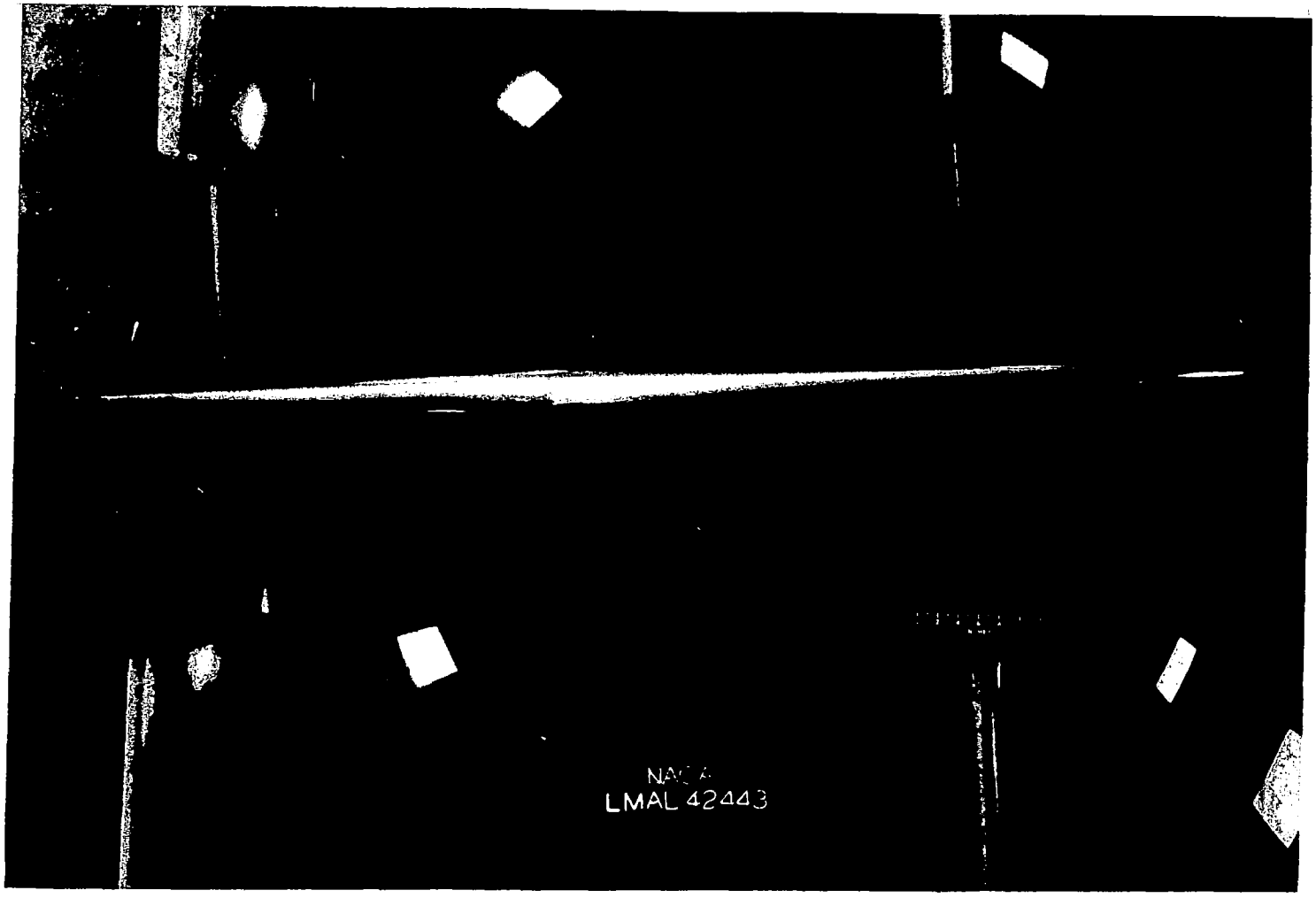

Figure 5.- Front view of inverted wing with image support struts installed for determination of strut tare forces.

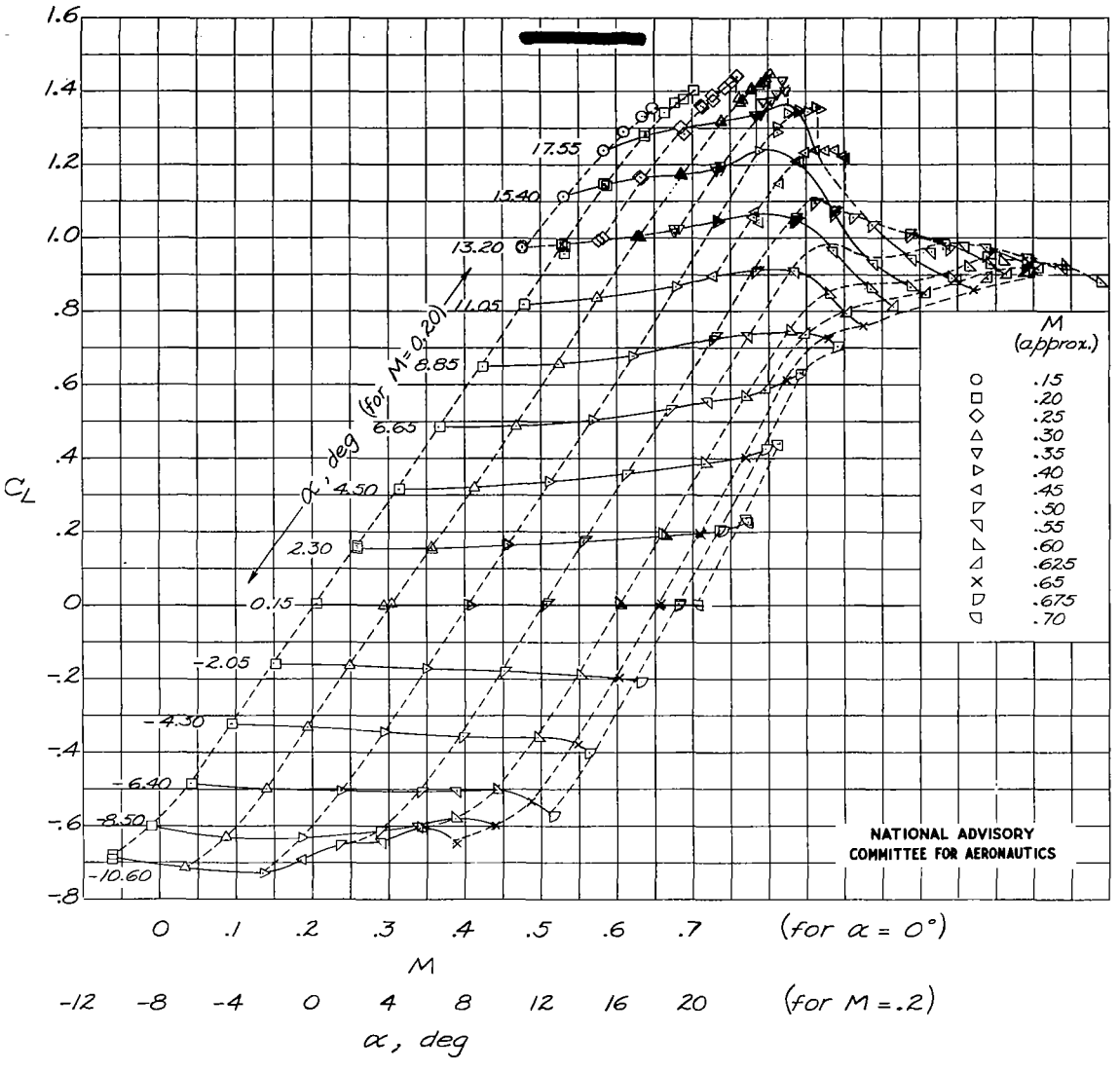

Figure 6.- Wing lift coefficient as a function of angle of attack and Mach number.

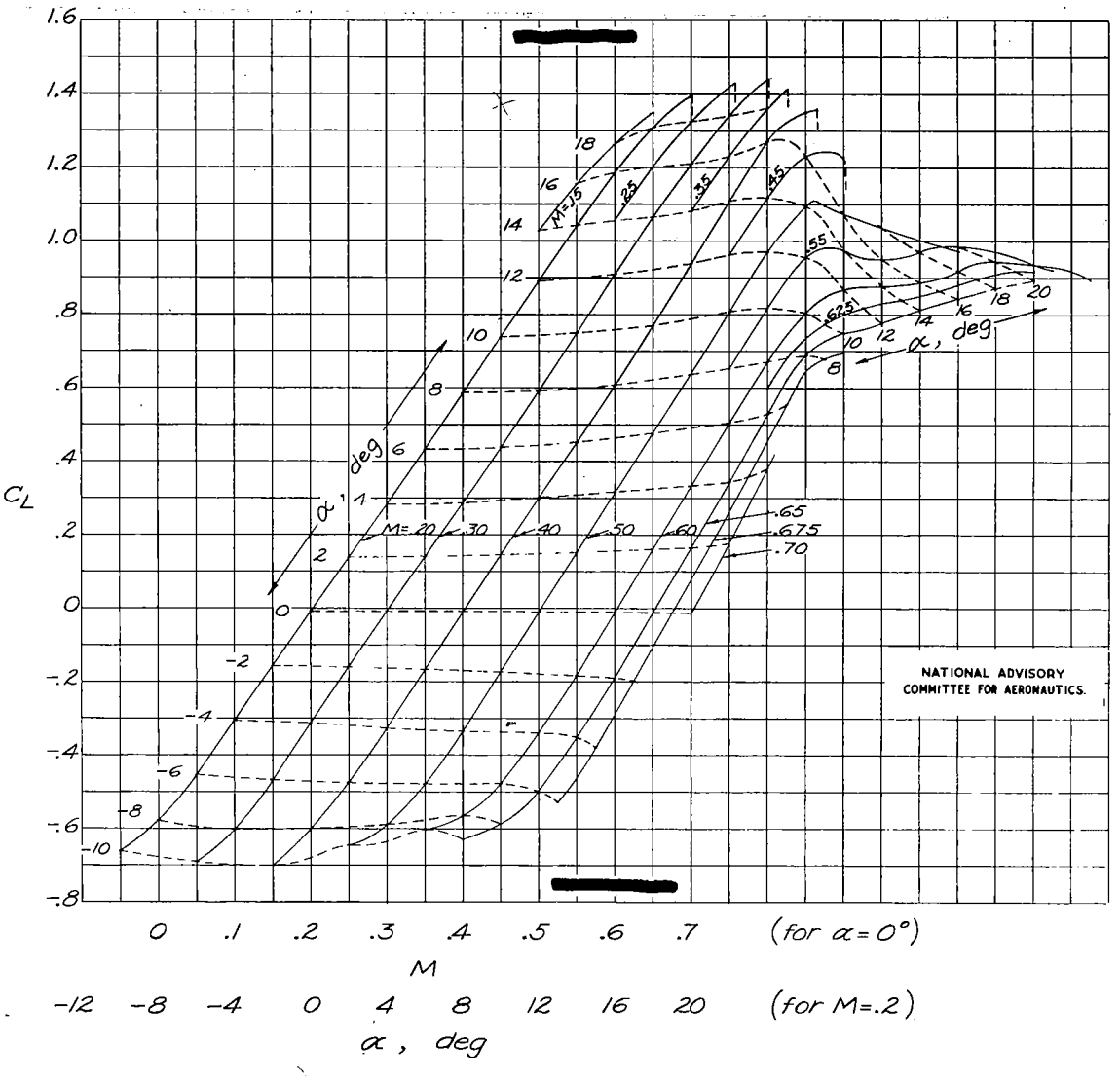

Figure 7.- Wing lift coefficient as a function of angle of attack and Mach number.

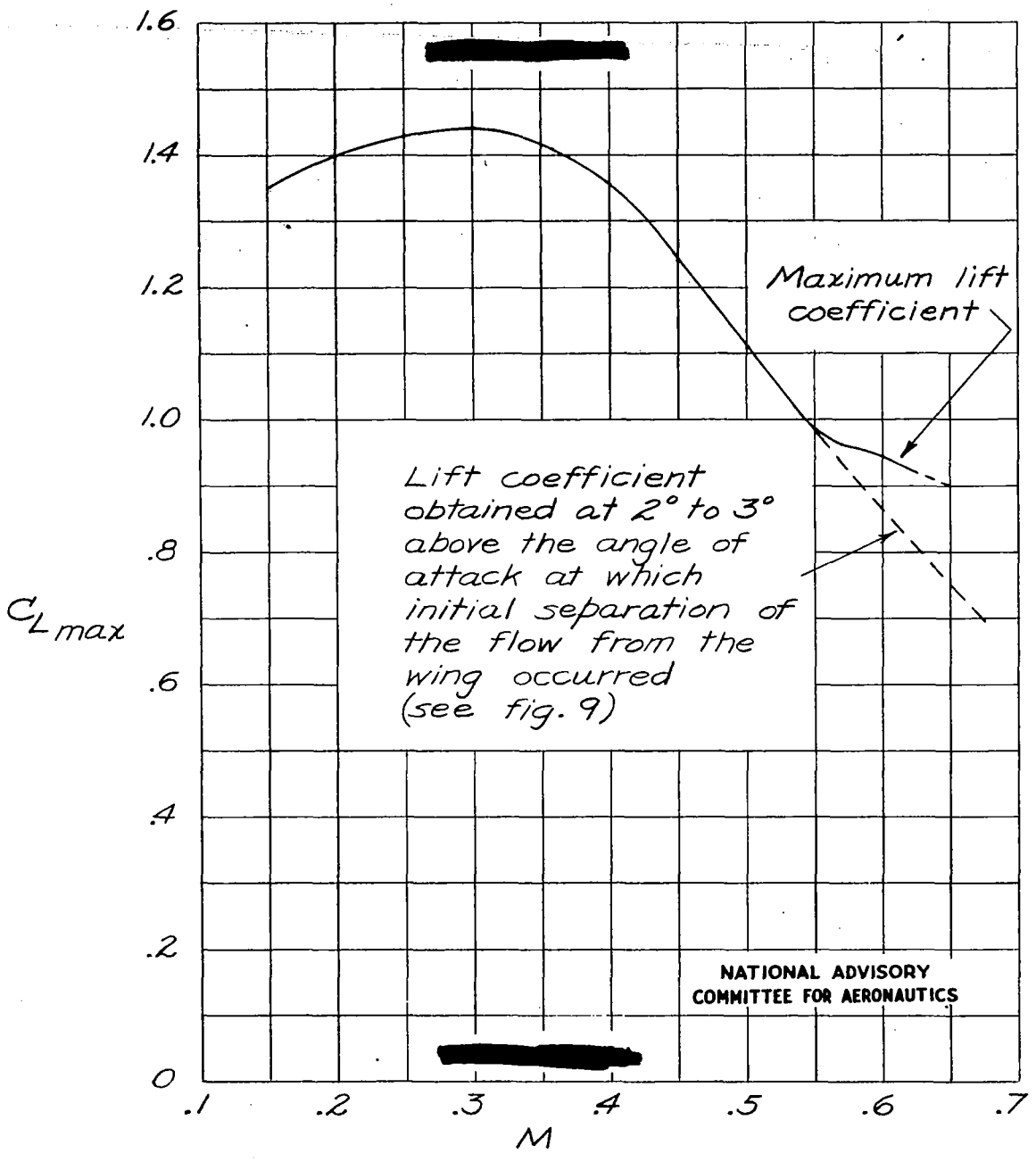

Figure 8.- Variation of wing maximum lift coefficient with Mach number.

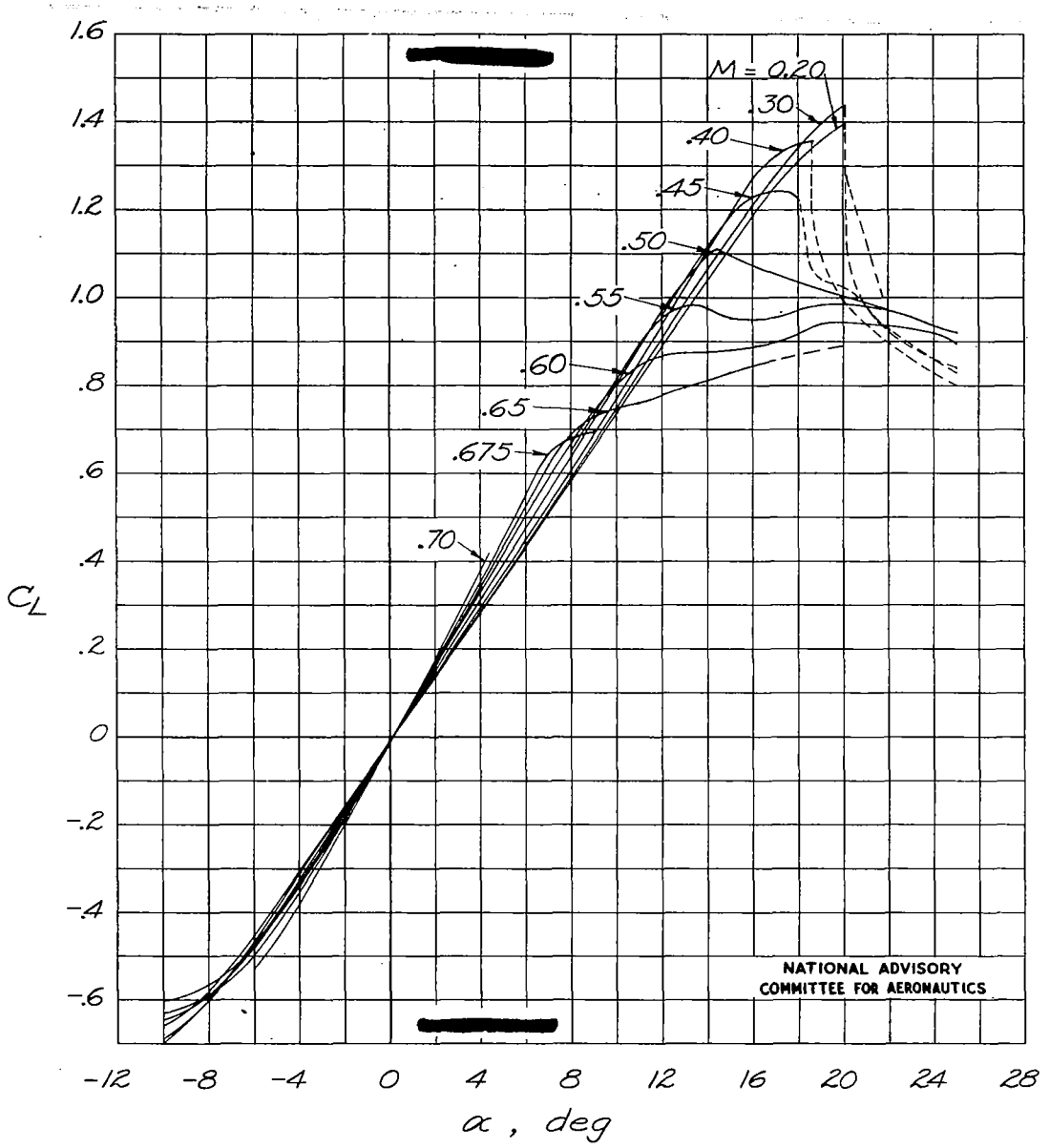

Figure 9.- Variation of wing lift coefficient with angle of attack for several Mach numbers.

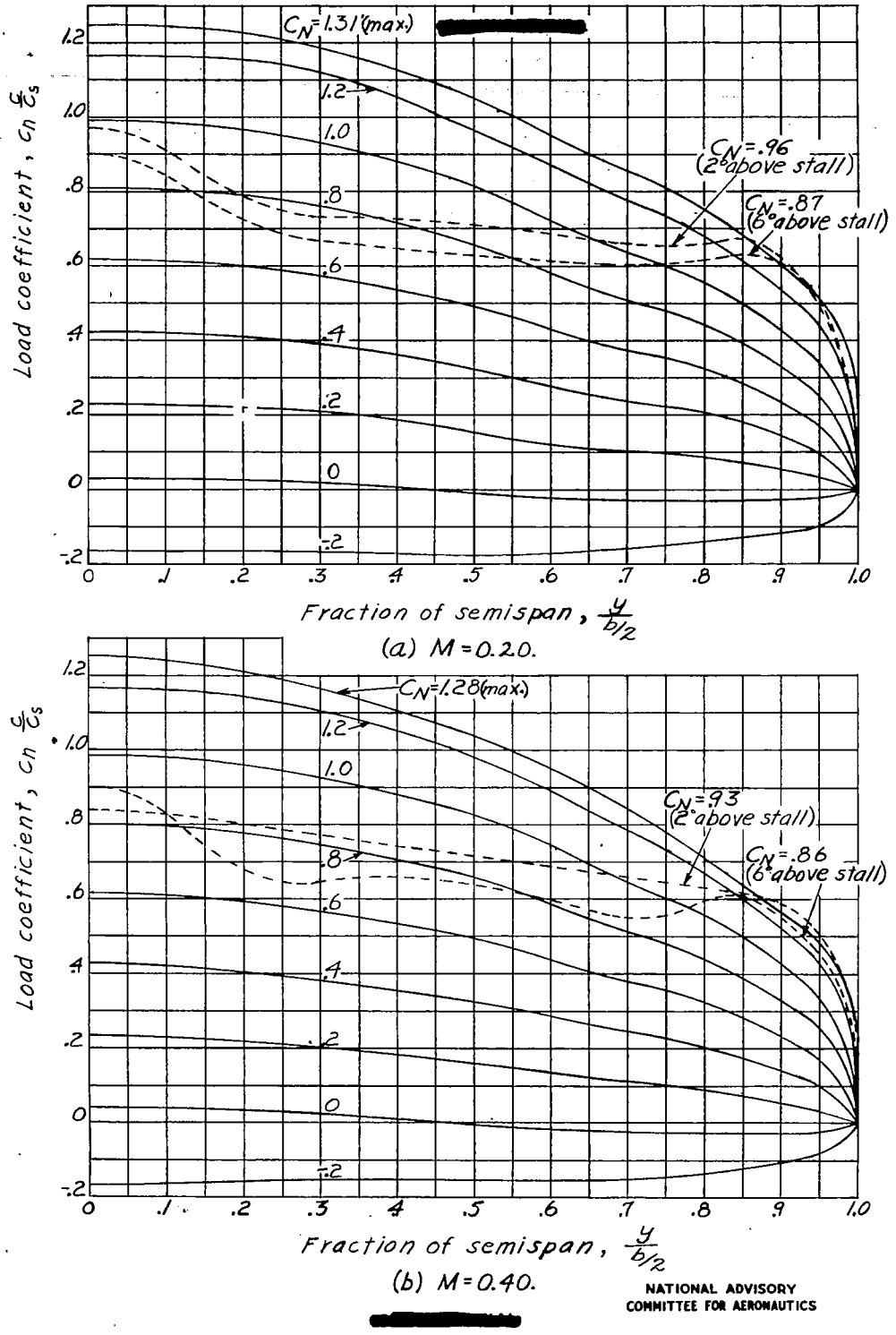

Figure 10. — Spanwise load distribution curves for several values of wing normal-force coefficient and Mach number.

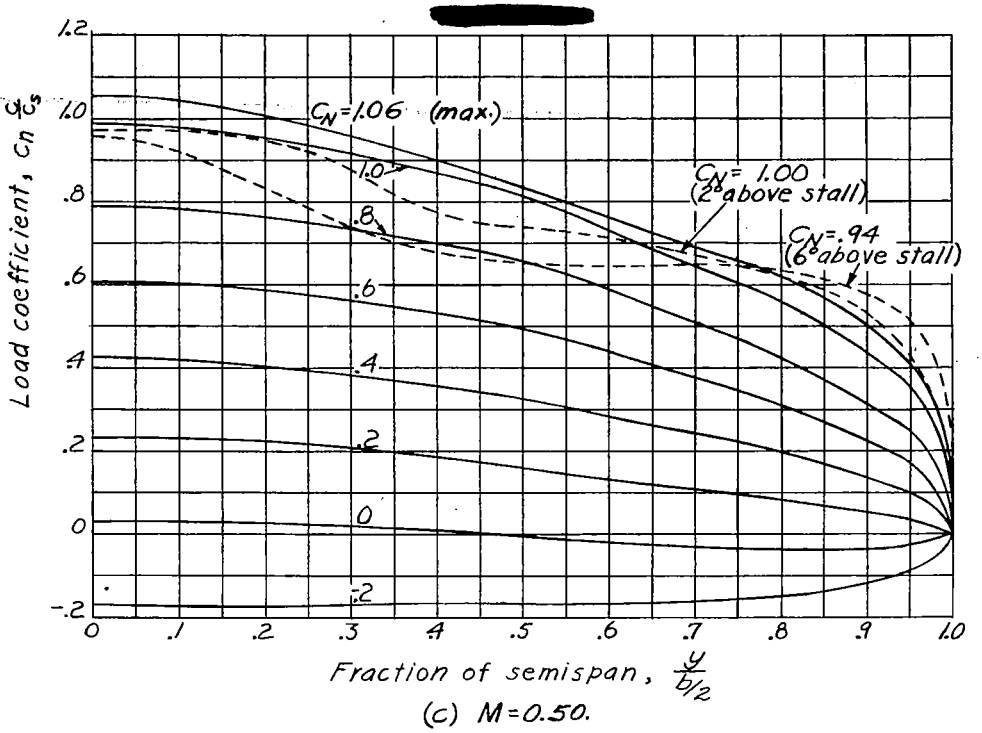

(c) M=0.50.

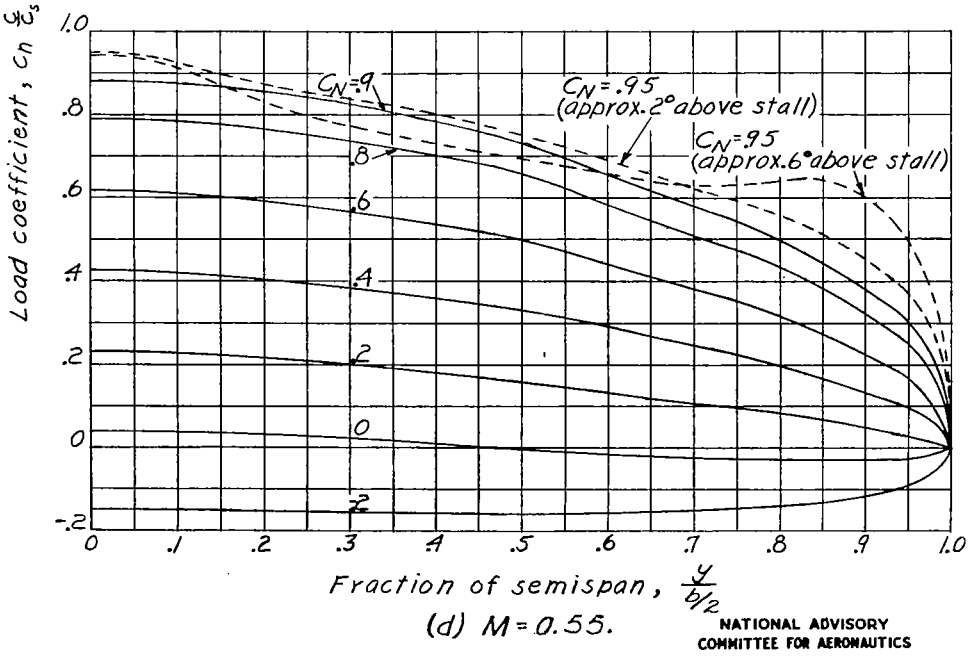

(d) M=0.55.

NATIONAL ADVISORY COMMITTEE FOR AERONAUTICS

Figure 10.- Continued.

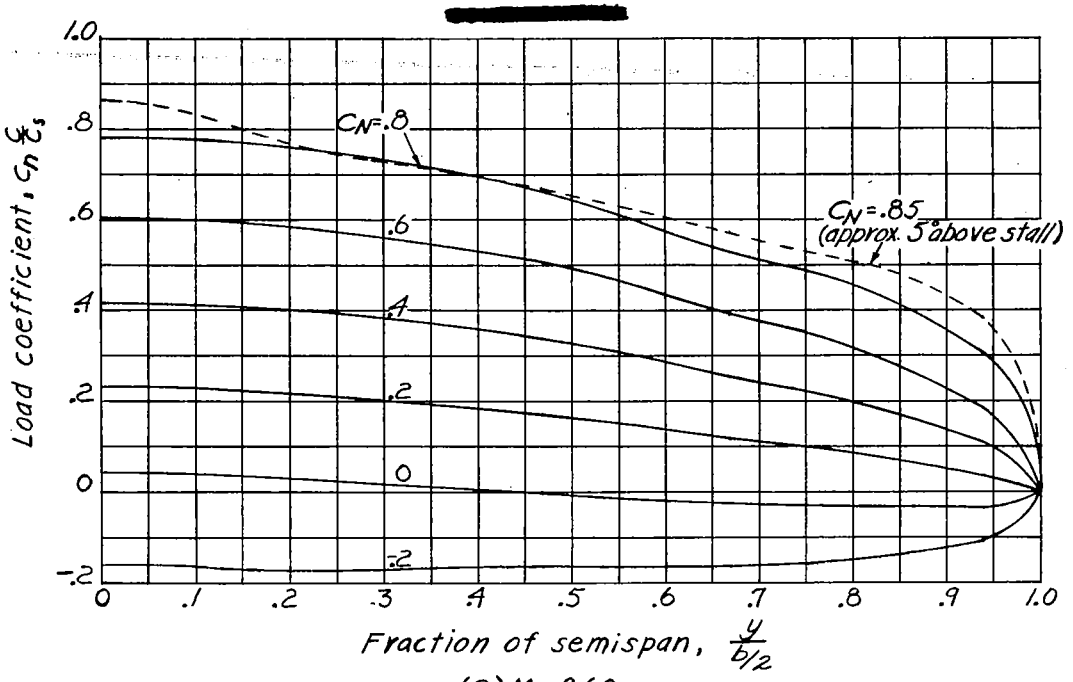

(e) M=0.60.

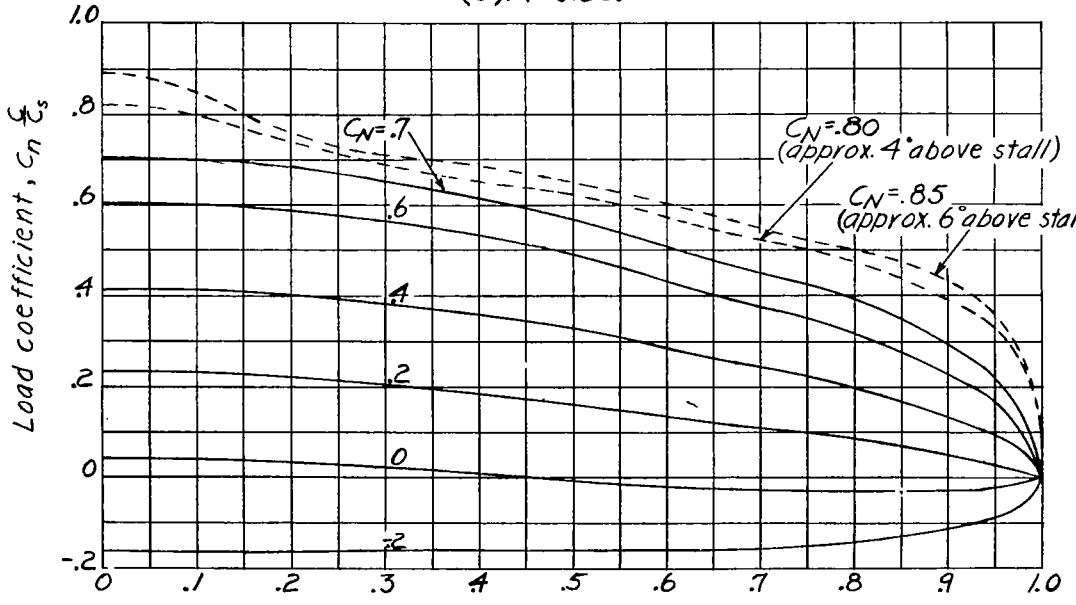

(f) M=0.625.

NATIONAL ADVISORY COMMITTEE FOR AERONAUTICS

Figure 10. - Continued.

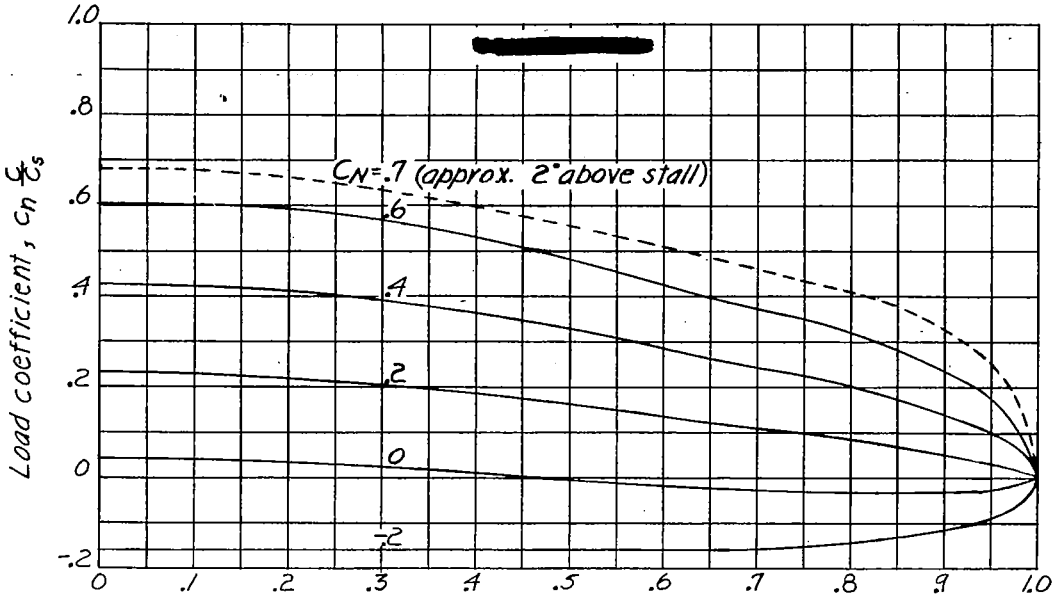

(g) M = 0.65.

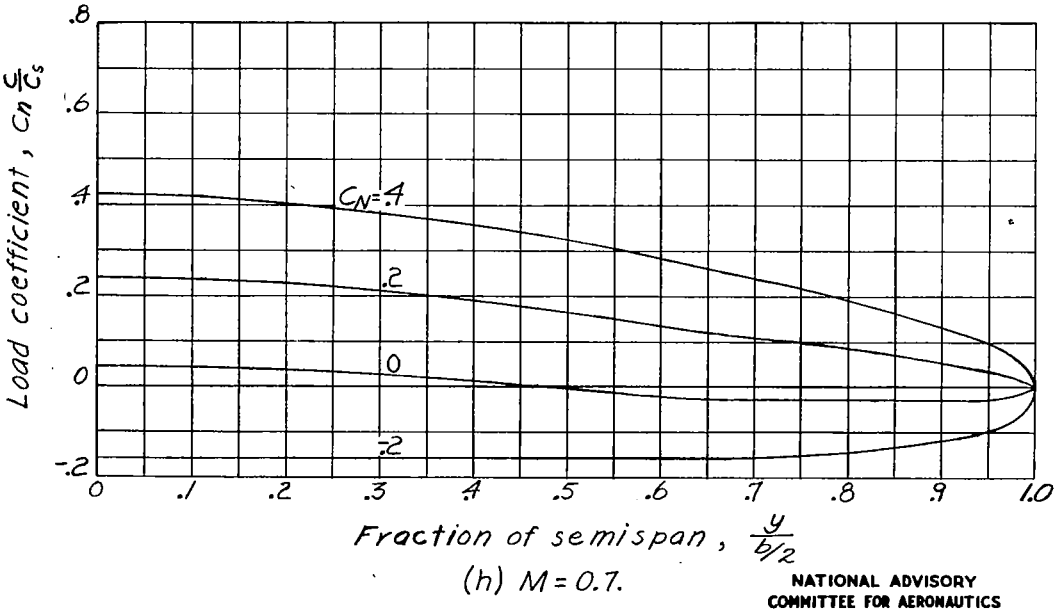

(h) M = 0.7.

NATIONAL ADVISORY COMMITTEE FOR AERONAUTICS

Figure 10. - Concluded.

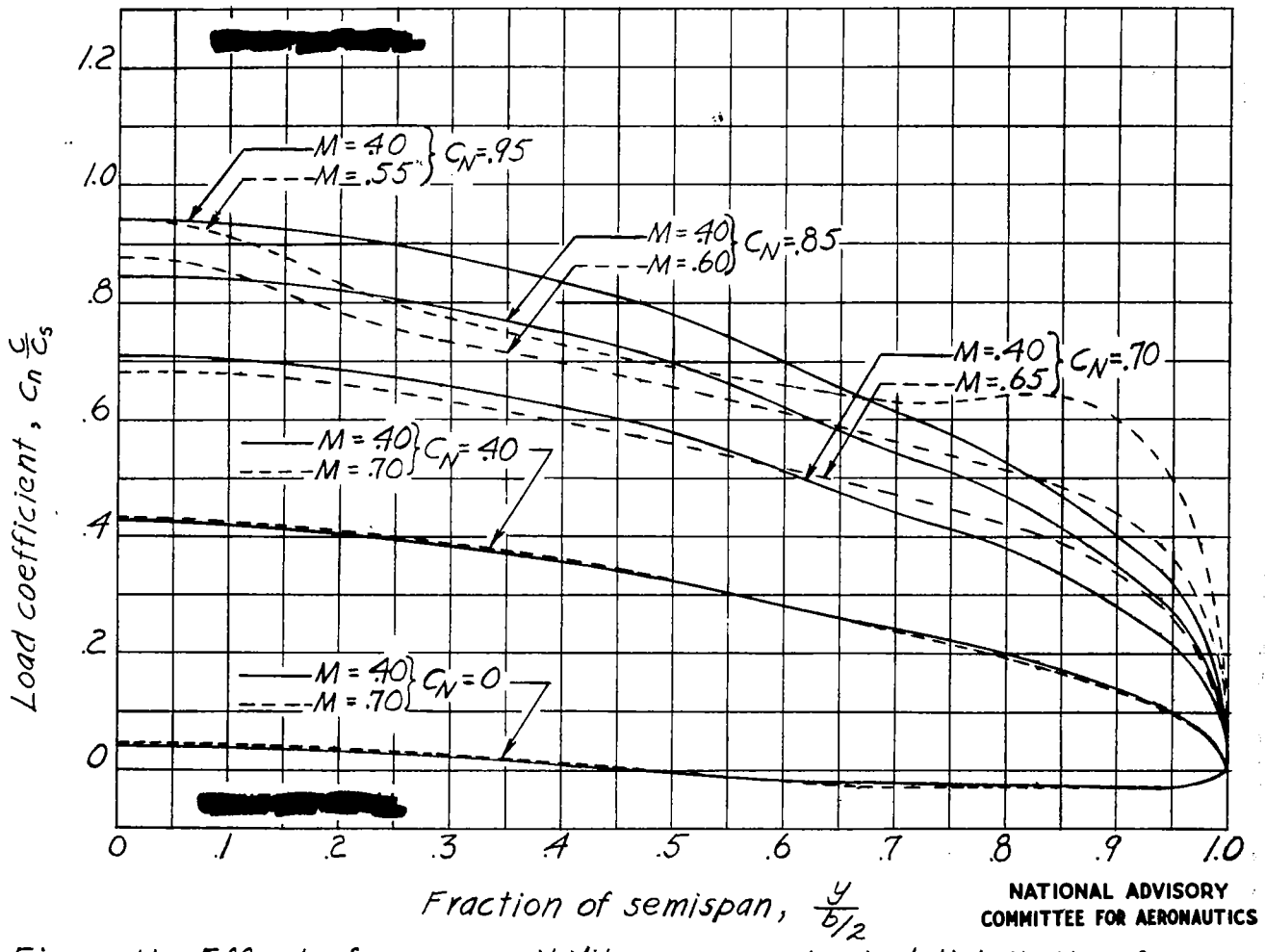

Figure 11.- Effect of compressibility on spanwise load distribution for several values of wing normal-force coefficient.

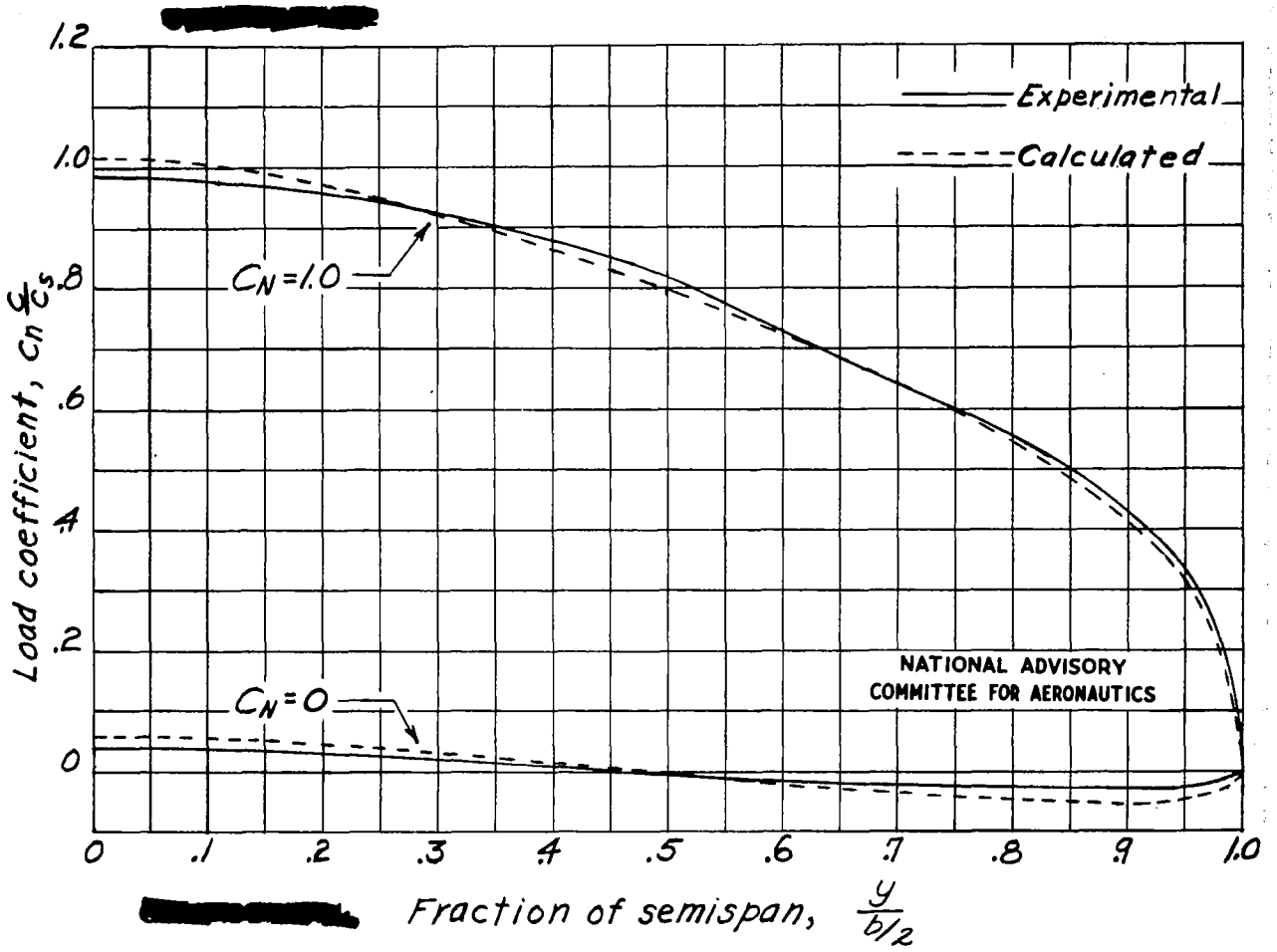

Figure 12.- Comparison of experimental and calculated load distribution curves for wing normal-force coefficients of 0 and 1.0 at M = 0.40.